ISSN 0023-1584, Kinetics and Catalysis, 2010, Vol. 51, No. 4, pp. 548–558. © Pleiades Publishing, Ltd., 2010.
Original Russian Text © F.A. Yandieva, M.V. Tsodikov, A.V. Chistyakov, V.Ya. Kugel', Ya.V. Zubavichus, A.A. Veligzhanin, L.E. Kitaev, V.V. Yushchenko, A.E. Gekhman, I.I. Moiseev, 2010, published in Kinetika i Kataliz, 2010, Vol. 51, No. 4, pp. 572–582.

Alumina–Platinum Catalyst in the Reductive Dehydration of Ethanol and Diethyl Ether to Alkanes

F. A. Yandieva[a], M. V. Tsodikov[a], A. V. Chistyakov[a], V. Ya. Kugel'[a], Ya. V. Zubavichus[b], A. A. Veligzhanin[b], L. E. Kitaev[c], V. V. Yushchenko[c], A. E. Gekhman[d], and I. I. Moiseev[a]

[a] *Topchiev Institute of Petrochemical Synthesis, Russian Academy of Sciences, Moscow, 119991 Russia*
[b] *Kurchatov Institute Russian Research Center, Moscow, 123182 Russia*
[c] *Moscow State University, Moscow, 119899 Russia*
[d] *Kurnakov Institute of General and Inorganic Chemistry, Russian Academy of Sciences, Moscow, 117901 Russia*
e-mail: yand@ips.ac.ru

Received July 27, 2009

Abstract—The reductive dehydration of ethanol and diethyl ether selectively occurs with the formation of alkanes to C_{10+} on an AP-64 alumina–platinum catalyst (0.6 wt % Pt/γ-Al_2O_3) after its reduction with hydrogen at 450°C for 12 h in Ar. It was found that one of the main reaction paths is the insertion of ethylene into substrate intermediates with the predominant formation of normal alkanes. It was found by XAFS spectroscopy that Pt_2Al intermetallide particles were formed along with platinum metal clusters after long reduction. The ammonia TPD data indicated a change in the acid properties of the surface after the long reduction of the catalyst: the concentration of medium-strength surface aprotic acid sites increased by a factor of 2. It was found that the interaction of aprotic sites with water vapor resulted in the formation of strong proton acid sites. It is likely that these latter are responsible for the growth of a carbon skeleton in the course of alkane formation from ethanol.

DOI: 10.1134/S0023158410040142

INTRODUCTION

Aluminum oxide is a well-known catalyst for acid-catalyzed reactions [1]. In the contact of ethanol with Al_2O_3 at elevated temperatures, the substrate is dehydrated to form ethylene and diethyl ether (DE). Recently, it was demonstrated that an alumina–platinum catalyst exhibits the same acid properties [2–4]. We found that, upon heating in an atmosphere of hydrogen, a commercial alumina–platinum catalyst (AP-64) gains the capacity to catalyze the crosslinking of the carbon skeletons of ethanol molecules with the elimination of water and the formation of alkanes:

$$m C_2H_5OH + 2[H] \longrightarrow C_nH_{2n+2} + mH_2O. \quad (I)$$

This reaction, which is known as the reductive dehydration of alcohols, was studied previously in the presence of intermetallides and a fused iron catalyst [5–7].

This work was devoted to reaction (I) catalyzed by an alumina–platinum catalyst thermally treated in an atmosphere of hydrogen and to the transformations of this catalyst in the course of thermal treatment.

EXPERIMENTAL

The AP-64 commercial alumina–platinum catalyst (~0.6 wt % Pt/γ-Al_2O_3; specific surface area, ~200 m^2/g; pore volume, 0.65 cm^3) was used in this study. Ethanol of analytical grade was used without preliminary purification. The conversion of ethanol was studied in laboratory flow-circulation and flow systems with a fixed catalyst bed [3]. Standard experiments were performed in an atmosphere of argon at 350°C, 50 atm, alcohol supply space velocity $V = 0.5\ h^{-1}$, and gas circulation rate of 50 cm^3/min. To determine the effects of temperature and gas space velocity on the yield of reaction products, they were varied over the ranges of 250–400°C and 0.4–1.7 h^{-1}, respectively. Before performing an experiment, the catalyst was activated at 100, 300, and 450°C and 50 atm for 10–12 h in a flow of hydrogen (10–30 l/h). After completion of the activation, the reactor was thoroughly purged with argon.

Ethanol was supplied to an evaporator with a high-precision syringe pump (HPP 5001); alcohol vapor from the evaporator arrived at a reactor. The reaction products arrived at a cooled gas–liquid separator; then, the condensed liquid fraction was collected in a receiver. A mixture of argon with uncondensed products was returned to the reaction volume of the system with the use of a circulation pump.

Gaseous reaction products were analyzed by on-line gas chromatography. The C_1–C_5 hydrocarbon gases were determined on a Kristall-4000 chromatograph: flame-ionization detector (FID); carrier gas, helium (70 cm^3/min); $T_{col} = 120$°C; $P = 1.65$ MPa; HP-PLOT/Al_2O_3 column, 50 m × 0.32 mm.

Analysis for CO, CO_2, and H_2 was performed on a Kristall-4000 chromatograph: thermal-conductivity detector; carrier gas, high-purity argon (30 ml/min); SKT column, 150 m × 0.4 cm; $T_{col} = 130°C$. Low concentrations of CO (<0.4 vol %) were determined using a Riken Keiki gas analyzer with an IR cell (Model RI-550A).

Liquid organic reaction products in aqueous and organic phases were identified using MSD 6973 (Agilent) and Automass-150 (Delsi Nermag) GC–MS instruments: EI = 70 eV; sample volume, 1 μl. First column: HP-5MS (0.32 mm × 50 m); $D_f = 0.52$ μm; heating from 50°C (5 min) at a rate of 10 K/min to 270°C; $T_{inj} = 250°C$; constant flow rate of 1 ml/min; split ratio, 1/(100–200). Second column: CPSil-5 (0.15 mm × 25 m); $D_f = 1.2$ μm; heating from 50°C (8 min) at a rate of 10 K/min to 270°C; $T_{inj} = 250°C$; $P_{inj} = 2.2$ bar; split ratio, 1/300. The concentrations of organic substances were quantitatively determined by GLC on a Varian 3600 instrument with a Chromtech SE-30 column of size 0.25 mm × 25 m; $D_f = 0.3$ μm; heating from 50°C (5 min) at a rate of 10 K/min to 280°C; $T_{inj} = 250°C$; $P_{inj} = 1$ bar; split ratio, 1/200; FID. Trifluoromethylbenzene was used as an internal standard for the organic layer, and internal normalization was used for the aqueous layer. The ethanol content of the aqueous phase was determined by GC–MS from the ratio between the integral signals of the alcohol and water using the absolute calibration method.

The acid properties of the catalyst were studied by the temperature-programmed desorption (TPD) of ammonia, which was used as a probe molecule. A ~0.1-g sample (weighed to within 5×10^{-4} g) of the catalyst (a fraction of 0.25–0.50 mm) was placed in a quartz reactor on a bed of quartz with a particle size of 1.0–0.5 mm. The sample was heated in a flow of dry air to 500°C at a rate of 10 K/min and calcined at this temperature for 1 h in a flow of air and for 1 h in a flow of helium; thereafter, it was cooled to room temperature. Next, the sample was saturated with ammonia for 0.5 h in a flow of dry ammonia diluted with nitrogen (1 : 1). The physically adsorbed ammonia was removed at 100°C in a flow of dry helium for 1 h. Thereafter, the sample was sharply cooled in a flow of dry helium (30 ml/min) to room temperature by immersing the reactor in cold water; the system was connected to a detector (katharometer), and the temperature was linearly increased (~8 K/min) to 750°C in a flow of dry helium (30 ml/min). The experimental data were treated using the EKOKhROM analytical software. In each particular case, a curve of the TPD of ammonia in the temperature (°C)–rate of ammonia desorption (μmol g^{-1} s^{-1}) coordinates was a result of the experiment.

The NH_3 TPD data were treated by matching the experimental and calculated shapes of the curves in accordance with a published procedure [8]. This allowed us to find the total acidity and the distribution function of acid sites in terms of the activation energies of ammonia desorption over the range of activation energies from a minimum (E_{min}) to a maximum value (E_{max}) and to calculate the average value ($\langle E \rangle$), which characterizes the average acid strength of sites, for the entire range of desorption. The intervals of the activation energies of desorption were divided into equal portions (5 kJ/mol), within which the sites were considered uniform, and their strength was determined as the activation energy that corresponds to the center of a portion.

The local structure and charge state of platinum were studied by XAFS spectroscopy. The XANES and EXAFS X-ray absorption spectra for two catalyst samples (initial AP-64 alumina–platinum catalyst and the catalyst subjected to reductive treatment in hydrogen at 50 atm and 450°C for 12 h) and standard materials (platinum foil and the oxide and chloride derivatives of Pt^{2+} and Pt^{4+}) were measured at the Structural Materials Science station of the Kurchatov Center for Synchrotron Radiation and Nanotechnology [7]. The spectra were measured in the transmission mode using two ionization chambers filled with argon. A monoblock monochromator with a Si(111) cut was used for the monochromatization of a synchrotron radiation beam. To prepare a sample, catalyst powder was pressed into a pellet 1.5 mm thick in an atmosphere of H_2 or Ar; the pellet was covered with a thin polymer film and transferred to the spectrometer under anaerobic conditions. For each particular sample, three to four independent measurements were performed to check the reproducibility of the results.

The Athena and Artemis programs from the IFEFFIT package [9] were used for the treatment of the spectra, including normalization, atomic-like background discrimination, Fourier transform, and nonlinear matching procedures. The FEFF8 program [10] was used to calculate photoelectron scattering phases and amplitudes; the same program was used to theoretically calculate the XANES spectra of the structural models of catalysts. The nonlinear matching procedure was performed for a curve of normalized EXAFS values of $\chi(k)$ multiplied by k^3 over the range of $k = 2–15$ $Å^{-1}$.

The phase composition of the alumina–platinum catalyst was studied by X-ray diffraction analysis on a computer-controlled DRON-3M instrument over the 2θ angle range of 20°–80°. Filtered CuK_α radiation was used. A 2 × 4 slit was used to restrict an X-ray beam at the outlet of the X-ray tube. The measurement was performed with sample rotation.

RESULTS AND DISCUSSION

Catalytic Activity and Selectivity of Pt/γ-Al_2O_3 in the Reductive Dehydration of Ethanol

In the flow system, the commercial alumina–platinum catalyst mainly performed the dehydration of ethanol over a range of 250–400°C; the yield of ethane

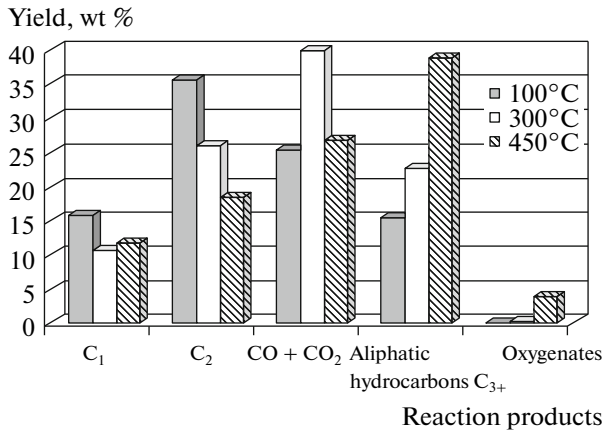

Fig. 1. Effect of the reduction temperature of Pt/Al_2O_3 on the composition of ethanol conversion products.

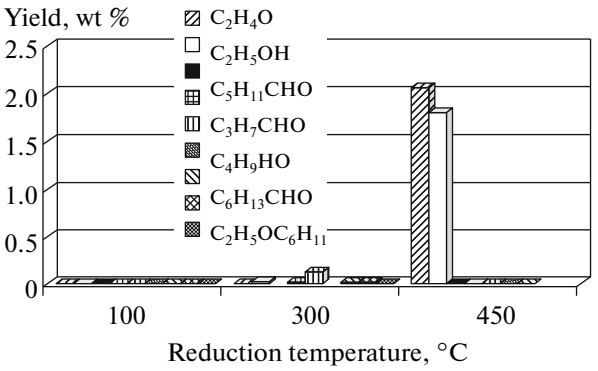

Fig. 2. Composition of oxygenates obtained from ethanol on AP-64 reduced at various temperatures.

was negligibly low [2–4]. The treatment of AP-64 with hydrogen even at a moderate temperature (100°C) noticeably changed the properties of the catalyst. Thus, ethanol was mainly converted into gaseous products C_1–C_4, CO, and CO_2 (75 wt %) (Fig. 1).

The character of ethanol transformations in the presence of a catalyst prereduced at 450°C changed even more dramatically. The yield of methane decreased, and the yield of higher molecular weight alkanes from C_3 to C_{12} increased. In addition to alkanes, acetaldehyde, ethers, and hexanol were present in small amounts in the liquid products (Figs. 1 and 2; Table 1).

The reductive dehydration of ethanol occurs over a narrow range of temperatures and ethanol space velocities. It was found that a temperature of 300–350°C and an ethanol space velocity from 0.4 to 0.9 h^{-1} are optimum conditions for ethanol conversion into alkanes. At a temperature lower than 300°C and a space velocity higher than 0.9 h^{-1}, a noticeable loss of selectivity for alkane formation occurred (Figs. 3a, 3b).

Process conditions also had a considerable effect on the yield of alkanes. Table 1 summarizes the composition of ethanol conversion products in the presence of the γ-Al_2O_3 support, which was used for the preparation of an alumina–platinum catalyst, and AP-64 under flow and flow-circulation conditions. As can be seen, in the presence of only alumina in the circulation mode (60% ethanol conversion), ethylene (30.2 wt %) and diethyl ether (4.5%) were the main reaction products. The gaseous reaction products also contained a small amount of butylenes; it is likely that they were formed by the dimerization of ethylene.

Under flow-circulation conditions on Pt/γ-Al_2O_3, ethanol was mainly converted into C_3–C_{12} alkanes, whose total yield was 36.9%; in this case, the total yield

Table 1. Yields of the products of ethanol and diethyl ether conversion (wt %) depending on experimental conditions (T = 350°C, P = 8 atm, Ar)

Products	Ethanol			Diethyl ether	
	flow circulation		flow	flow circulation	flow
	γ-Al_2O_3	Pt/γ-Al_2O_3	Pt/γ-Al_2O_3	Pt/γ-Al_2O_3	Pt/γ-Al_2O_3
H_2	0.06	0.1	1.4	0.1	0.6
CH_4	0.03	12.3	7.2	7.9	6.6
C_2H_6	0.48	19.3	9.8	24.3	4.7
C_2H_4	30.2	–	14.1	2.7	8.6
CO	–	6.7	42.1	6.3	29.9
CO_2	–	21.2	–	15.9	29.1
n-Alkanes C_3–C_{12}	C_4H_{10}–0.09	33.1	14.2	30.3	7.6
Isoalkanes C_4–C_{12}	–	3.8	–	2.0	–
Alkenes C_3–C_{12}	C_3H_6–0.44 C_4H_8–0.44	2.3	5.8	8.3	4.5
Cycloalkanes	–	0.8	–	–	–
Aromatics	–	0.4	3.8	0.5	1.3
Oxygenates	4.50 [$(Et)_2O$]	–	1.3	3.7	7.3

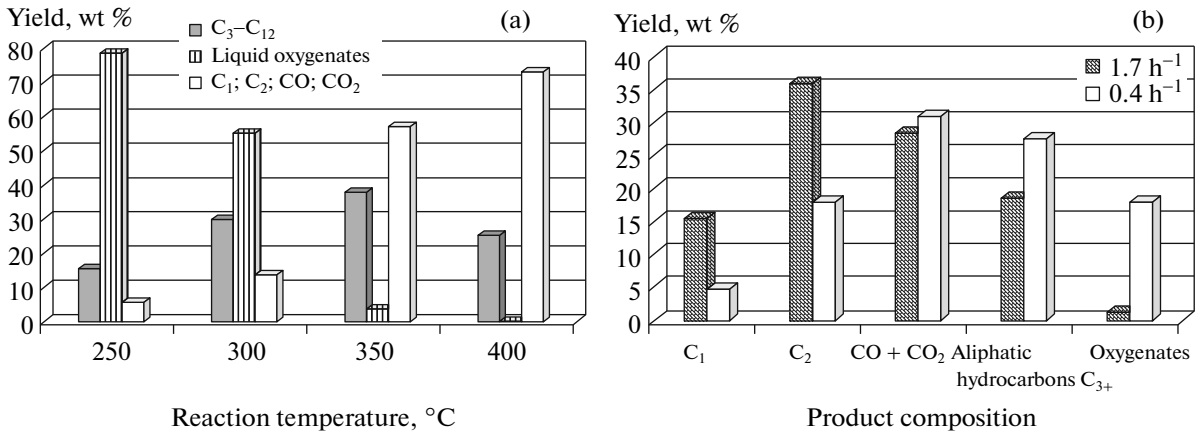

Fig. 3. Effects of (a) reaction temperature and (b) space velocity on the composition of ethanol conversion products.

of aliphatic hydrocarbons was 39.2% (Table 1). Table 1 indicates that the gaseous products contained a considerable amount of carbon oxides and C_1 and C_2 alkanes. The liquid products contained small amounts of cycloalkanes, olefins, and aromatic hydrocarbons, the total concentration of which was no higher than 1.5%, along with alkanes.

In the conversion of ethanol under flow conditions, the yield of C_{3+} aliphatic hydrocarbons decreased to 20%, and the concentration of C_2 and C_{3+} olefins noticeably increased; ethylene was predominant among these olefins (Table 1).

The formation of considerable amounts of ethylene upon the reductive dehydration of ethanol under flow conditions suggests that a change of the reaction to flow-circulation conditions facilitates the return of ethylene to the reaction zone to generate conditions for its participation in the synthesis of aliphatic hydrocarbons.

Note that the conventional contact time of gaseous reaction products with the active catalyst surface in the course of the process performed under flow-circulation conditions increased from 9.6 (flow conditions) to 1152 s during the experiment time (3.5 h). It is most likely that this facilitated the deeper development of condensation processes (oligomerization and aldol condensation) and, consequently, increased the yield of C_3–C_{12} alkanes (Table 1).

Thus, the experimental data suggest that ethylene and acetaldehyde, which result from the dehydration and dehydrogenation of ethanol in the course of alkane formation (see previous section), can serve as reaction intermediates in the growth of a hydrocarbon chain. In terms of this hypothesis, it is likely that ethylene undergoes oligomerization at acid sites to result in the predominant formation of normal alkanes. The reaction paths of chain growth with the participation of acetaldehyde are also well known [11, 12]. One of these reaction paths is the reaction discovered by Ostromyslenskii [11], in which acetaldehyde reacts with ethanol to form butadiene, which undergoes copolymerization with ethylene at the subsequent step. The reaction path of branched hydrocarbon chain growth due to an aldol condensation is also possible [13].

Performing the reaction of ethanol under flow-circulation conditions, we managed to identify acetaldehyde and ethylene in very small amounts. This was likely due to the high reactivity of them in the test reactions.

Role of Ethylene and Acetaldehyde as Reaction Intermediates in the Reductive Dehydration of Ethanol

To test the hypothesis on the participation of ethylene and acetaldehyde in hydrocarbon chain growth, we performed experiments in the presence of the alumina–platinum catalyst, in which various ethylene and acetaldehyde amounts were introduced into the reaction zone.

From Table 2, it follows that the yield of C_4–C_{10} alkanes noticeably increased as the amount of ethylene in the reaction mixture was increased.

Table 3 indicates that, along with the growth of hydrocarbons with even numbers of carbon atoms, their yield increased with respect to the yield of hydro-

Table 2. Effect of ethylene on the yield of aliphatic hydrocarbons with even numbers of carbon atoms in the reductive dehydration reaction of ethanol

Amount of ethylene added,* mmol	Relative molar amounts of the resulting alkanes			
	C_4	C_6	C_8	C_{10}
0	1.00	1.00	1.00	1.00
15	1.96	0.88	1.15	1.91
60	2.06	1.23	1.75	2.33

* Ethylene was added to 0.7 mol of ethanol supplied in the reaction time.

Table 3. Ratio of the yield of hydrocarbons containing even numbers of carbon atoms to the yield of hydrocarbons containing odd numbers of carbon atoms in the reductive dehydration products upon the addition of ethylene to the reaction volume

Hydrocarbon ratio	Ethylene amount added to the starting ethanol, mmol		
	0	15	60
C_4/C_5	4.48	8.81	9.22
C_6/C_5	6.78	5.96	8.33
C_8/C_5	1.49	1.72	2.61
C_{10}/C_5	0.12	0.23	0.27
C_4/C_7	7.16	14.07	14.73
C_6/C_7	10.83	9.53	13.30
C_8/C_7	2.39	2.74	4.17
C_{10}/C_7	0.19	0.36	0.44

carbons containing odd numbers of carbon atoms, C_5 and C_7.

Note the character of changes in the yield of hexane and its isomers upon the addition of ethylene to the converted ethanol. Upon the introduction of 2.2 mol % ethylene into the reactor, the yield of C_6 hydrocarbons insignificantly decreased (~10%). In the case of the addition of 8.3 mol % ethylene to the starting ethanol, the yield of C_6 hydrocarbons increased by only 20%. At the same time, the yield of other homologs containing even numbers of carbon atoms increased by a factor of almost 2. This fact suggests the high reactivity of C_6 hydrocarbons in the presence of ethylene toward the formation of C_8 and C_{10} higher homologs.

The formation of C_1–C_{9+} hydrocarbons with odd numbers of carbon atoms (Table 3) suggests that a parallel reaction path can occur, in which the resulting higher homologs of ethanol undergo dehydrogenation with the formation of aldehydes, which, in turn, undergo decarbonylation:

$$C_nH_{2n+1}OH \xrightarrow{-H_2} C_nH_{2n}O \longrightarrow CO + C_{n-1}H_{2(n-1)+2}, \quad \text{(II)}$$

where $n = 2$–12.

Note that ethylene was mainly converted into butylene and butane on the alumina–platinum catalyst in the absence of an alcohol. Consequently, the incorporation of ethylene into a hydrocarbon chain occurs efficiently only with the participation of the intermediates of the reductive dehydration of ethanol, which are formed on the catalyst surface.

The addition of acetaldehyde to the parent ethanol resulted in the formation of unidentified high-molecular-weight tarry oxygenates, whereas the composition of the hydrocarbon fraction remained almost unchanged.

Thus, the experimental results suggest that the incorporation of ethylene is one of the main reaction paths in the growth of a hydrocarbon skeleton in the reductive dehydration reaction of ethanol in the presence of the alumina–platinum catalyst containing an acid support.

Diethyl Ether Conversion under Reductive Dehydration Conditions

Previously, the formation of diethyl ether in the course of the reductive dehydration of ethanol was considered a parallel reaction path in the conversion of ethanol on the acid sites of aluminum oxide [6]. However, in the presence of the alumina–platinum catalyst prereduced with hydrogen at 450°C for 12 h, diethyl ether, as well as ethanol, was converted into alkanes with the numbers of carbon atoms in chains up to C_{10} and a small amount of olefins (the total yield was as high as 40.7%). The composition of diethyl ether conversion products obtained on this catalyst under flow-circulation reaction conditions was very close to the composition of ethanol conversion products (Table 1). The only difference is that ethylene and oxygenates were formed in small amounts upon the conversion of diethyl ether and the olefin content of liquid hydrocarbons insignificantly increased.

Upon the reaction performed under flow conditions, the composition of diethyl ether, as well as ethanol, conversion products was dramatically different from the composition obtained upon the process performed under flow-circulation conditions: the yield of C_3 aliphatic hydrocarbons decreased to 12.1%, and the concentration of C_2 and C_{3+} olefins noticeably increased with the predominance of ethylene (Table 1).

The formation of C_1–C_4 alkanes from diethyl ether was described earlier [14]. It was found that diethyl ether in the presence of catalysts containing to 25% Group VIII noble metals supported on activated carbon underwent hydro/dehydrogenation processes resulting in the formation of C_1–C_4 alkanes. In addition to light alkanes, tetrahydrofuran and ethanol were also detected in the reaction products [14, 15].

The formation of aliphatic hydrocarbons with the number of carbon atoms greater than four from diethyl ether was previously unknown.

Unlike previous publications [14, 15], we did not detect tetrahydrofuran in the products of diethyl ether conversion in the presence of the alumina–platinum catalyst.

Thus, the experimental results indicate that the commercial alumina–platinum catalyst subjected to long reduction at an elevated temperature exhibited unusual activity and selectivity in the transformations of ethanol and diethyl ether with the formation of C_3–C_{10+} alkanes, whose yield was as high as 38–40 wt % at a >80% concentration of a C_{5+} fraction in the liquid product.

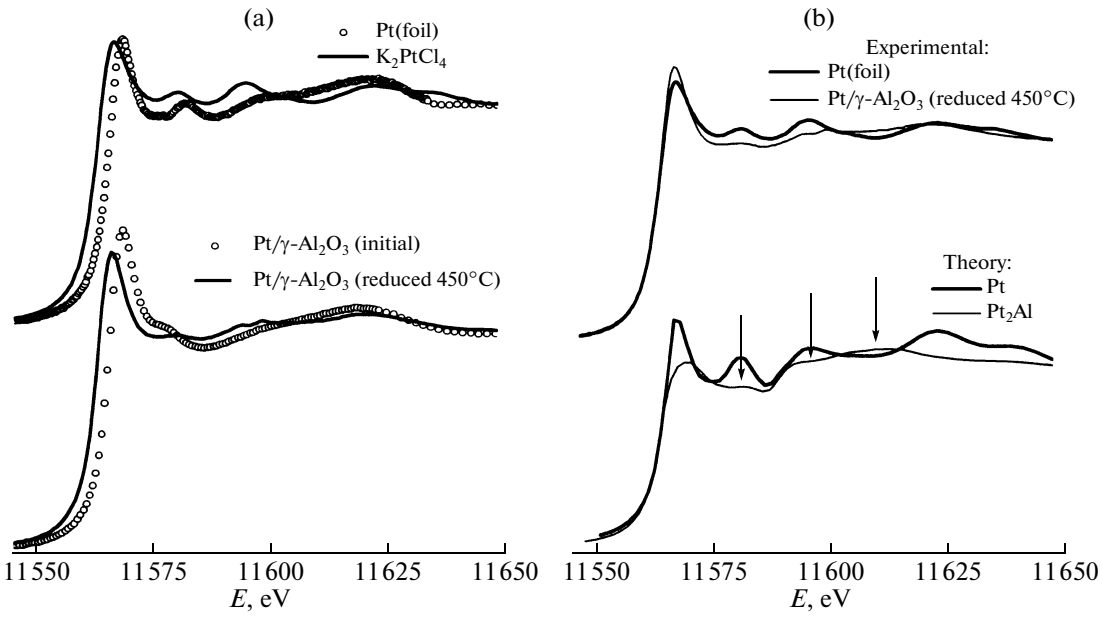

Fig. 4. Experimental XANES spectra at the L_3 edge of Pt for (a) initial and reduced AP-64 catalysts as compared with the spectra of standard substances (Pt foil and K_2PtCl_4) and (b) a comparison of the experimental spectrum of the reduced catalyst with the results of theoretical calculations for platinum metal and the Pt_2Al intermetallide [16].

In the reaction products, the ratio between normal alkanes and isoalkanes was 10 : 1 unlike 1 : 9, which was observed in the presence of the polymetallic catalytic composition $[TiFeZrMo]H_{0.18}$ + $Pt/\gamma\text{-}Al_2O_3$ [3]. This indirectly supports the conclusion on the reactions of ethylene with the intermediates of reductive ethanol dehydration.

Hydrogen was present in the gaseous reaction products of ethanol and diethyl ether conversion (Table 1). By analogy with published data [3], hydrogen, which is required for alkane formation according to the stoichiometry of reaction (I), can be supplied by the following reactions:

$$C_2H_5OH \longrightarrow CH_4 + CO + H_2; \quad \text{(III)}$$

$$CO + H_2O \longrightarrow CO_2 + H_2; \quad \text{(IV)}$$

$$C_2H_5OH + H_2O \longrightarrow 2CO + 4H_2. \quad \text{(V)}$$

The high concentration of carbon oxides in the products of diethyl ether conversion suggests that not only the above reactions of the formation of hydrogen, which is consumed for the hydrogenation of unsaturated hydrocarbons at platinum-containing sites (Table 1), but also the following reactions leading to the formation of ethylene are probable:

$$(C_2H_5)_2O \longrightarrow CH_4 + CO + C_2H_4 + H_2; \quad \text{(VI)}$$

$$(C_2H_5)_2O + H_2O \longrightarrow C_2H_4 + 2CO + 4H_2. \quad \text{(VII)}$$

It is most likely that the predominance of carbon dioxide was due to the occurrence of water gas reaction (IV), which is well known to intensely occur in the presence of an alumina–platinum catalyst [4].

Platinum-Containing Sites According to XAFS Spectroscopic Data

The experimental XANES spectrum (Fig. 4a) of the initial AP-64 alumina–platinum catalyst is characterized by a relatively low intensity white line with a spectral maximum at 11 569 eV (the white line in the XANES spectrum at the L_3 edge of Pt is formed by dipole-allowed $2p \longrightarrow 5d$ electron transitions; therefore, its intensity directly correlates with the number of vacancies in the $5d$ valence shell of platinum atoms, that is, with the formal oxidation number). The well-known spectra of the oxygen compounds of platinum(II) and platinum(IV) are characterized by much more intense white lines with spectral maximums shifted to higher energies. At the same time, the spectral maximum of platinum metal (see Fig. 4a) is even less intense and shifted toward lower energies. Of well-known spectroscopic standard substances, potassium chloroplatinate(II) is closest to the initial AP-64 catalyst in terms of both white line parameters and the near-edge fine structure over an energy range of 50–70 eV above the absorption edge. Most likely, that is to say that, before catalyst reduction, platinum atoms were mainly surrounded by chlorine atoms and the charge state of platinum was close to 2_+ (this preliminary conclusion is consistent with EXAFS data). The incomplete coincidence of the XANES fine structure of the initial AP-64 catalyst and K_2PtCl_4 suggests that the coordination polyhedron of platinum atoms in the commercial catalyst is different from a planar square, which occurs in K_2PtCl_4.

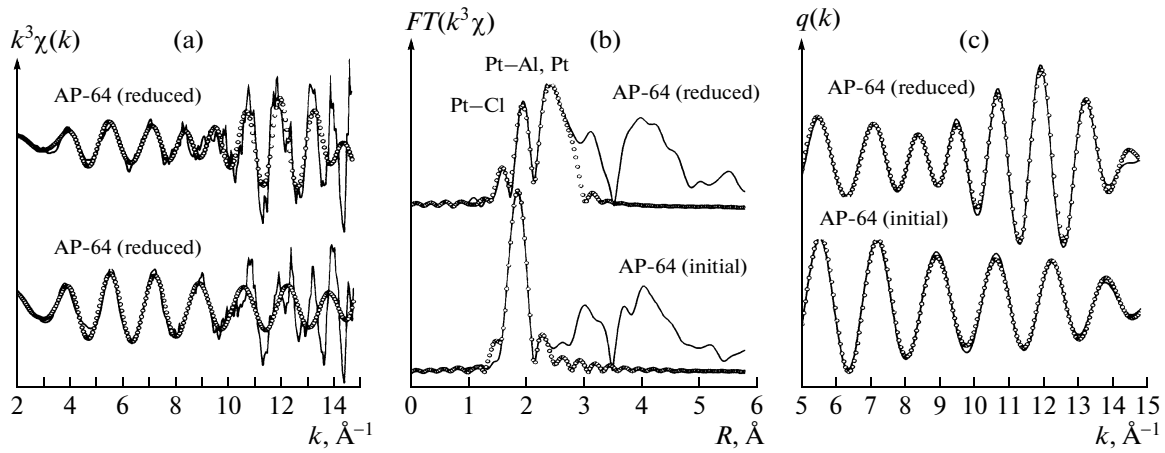

Fig. 5. Experimental EXAFS spectra at the L_3 edge of Pt for initial and reduced AP-64 catalysts (solid lines) and the results of the refining of structural models (points): (a) curves of the normalized EXAFS signal $k^3\chi(k)$, (b) curves after Fourier transform, and (c) curves obtained by inverse Fourier transform over the analyzed range of $q(k)$ distances.

Reductive treatment resulted in considerable changes in the XANES spectrum of the catalyst: the white line height somewhat decreased; the spectrum shifted by ~2 eV toward lower energies, and the fine structure of the spectrum changed. In this case, the shape of the spectrum approached that observed in platinum metal. Nevertheless, it is beyond reason to consider the complete coincidence of the spectra of the reduced catalyst and platinum metal. For a more detailed analysis of the possible electronic state and structure of platinum in the reduced catalyst, we performed a theoretical simulation of XANES spectra for platinum metal and a Pt_2Al alloy [16] using the FEFF8 program. Figure 4b shows the results of this simulation. It can be clearly seen that the observed differences between the experimental spectra of Pt and the reduced catalyst were adequately reproduced in the theoretical calculation for the Pt_2Al intermetallide and Pt metal (the most informative regions of the spectra are indicated by arrows in Fig. 4b). This result suggests the formation of direct platinum–aluminum contacts in the reduced catalyst.

Additional, more reliably interpreted information on the local atomic environment of platinum in catalysts can be obtained from an analysis of extended X-ray absorption fine structure (EXAFS) spectra. Figure 5 shows the pseudoradial distribution curves obtained by the Fourier transform of normalized EXAFS signals for the parent and reduced AP-64 catalyst samples, and Table 4 summarizes the refined values of local structure parameters.

It is most likely that, in the parent AP-64 catalyst, the coordination sphere of platinum atoms mainly contained chlorine atoms. The experimental curve was best consistent with the refined theoretical curve for a model with two nonequivalent Pt–Cl distances of 2.28 and 2.46 Å and the total coordination number of ~4. At great distances (3–5 Å), the Fourier-transformed spectrum exhibited relatively intense irregularly shaped peaks; this fact suggests that platinum atoms did not form isolated ion–molecule fragments but they were incorporated into a sufficiently rigid low-symmetry skeleton consisting of heavy atoms. A possible version can be the chemical grafting of platinum to the surface sites of γ-Al_2O_3 through one or two bridging chlorine atoms.

The Pt–Cl peak intensity considerably decreased after reductive treatment. Nevertheless, according to

Table 4. Effective coordination numbers (N) and interatomic distances (R) in the nearest environment of palladium atoms in the AP-64 alumina–platinum catalyst before and after reduction (according to EXAFS data)

Sample	Coordination sphere	N	R, Å	ΔE, eV	R_f^*
Initial	Pt–Cl	2.6	2.26	15.2	0.004
		1.1	2.43		
Reduced	Pt–O	0.4	1.97	12.9	0.038
(50 atm H_2, 450°C, 12 h)	Pt–Cl	0.8	2.29		
	Pt–Al	1.2	2.57		
	Pt–Pt	1.8	2.72		

*R_f is the reliability factor.

EXAFS data, chlorine atoms with an effective coordination number of <1 were retained in the coordination environment of platinum and oxygen atoms appeared at a Pt–O distance of 1.97 Å ($N = 0.4$); most likely, they suggest the formation of platinum bonds to support oxygen as chlorine ions were removed. The results of many previous studies [17–19] are indicative of the occurrence of oxidized platinum ionic species remained on the catalyst surface upon reduction.

Moreover, in the Fourier-transformed EXAFS spectrum of the reduced catalyst, a new intense peak appeared at $R \sim 2.5$ Å (with no phase correction), which is characteristic of direct metal–metal contacts (Fig. 5). The test of the possible combinations of Pt–Pt, Pt–Al, Pt–Pt, and Al contributions demonstrated that the appearance of this peak can be most likely explained by a combination of the contribution of Pt–Al and Pt–Pt contacts with interatomic distances of 2.57 and 2.72 Å, respectively, and the total coordination number of ~3. These interatomic distances and the coordination number ratios N(Pt–Al)/N(Pt–Pt) reliably indicate that the ultradispersed clusters (that, probably, consisted of a few atoms) of an aluminum–platinum alloy structurally similar to Pt_2Al were formed in the catalyst in the course of the severe reductive treatment. Note that the structure of long contacts at distances of 3–5 Å for the reduced catalyst differed only slightly from those observed in the parent catalyst.

Recently, by a combination of electron microscopy and XAS spectroscopy, it has been demonstrated that metal particles were formed on the surface of γ-Al_2O_3 after supporting the complex $[Pt(NH_3)_4(OH)_2 \cdot H_2O]$ without both thermal treatment and reduction. It was noted that subnanosized platinum particles are characterized by a narrow size distribution; they have the shape of a flattened drop and strongly interact with the support [20]. It was found that Pt_8Al_{21} aluminum–platinum alloy particles were formed in the course of reduction of the Pt/γ-Al_2O_3 catalyst at 800°C [21–23]. Petraszek et al. [24] used TEM to detect the particles of metastable Al_2Pt intermetallide, which were obtained upon the reduction of an alumina–platinum catalyst even at 500°C. At higher temperatures, ordered Pt_8Al_{21} intermetallides with an octahedral structure were also identified [24]. Petraszek et al. [24] hypothesized that, similarly to Rh ions, platinum was incorporated into the crystal structure of alumina, and then it underwent partial reduction. The ionic radius of Pt^{4+} is greater than the ionic radius of Al^{3+}. However, the possibility of this incorporation of platinum ions into the near-surface layers of alumina cannot be excluded.

Considering the mechanism of formation of platinum–aluminum intermetallides, Petraszek et al. [24] believed that, at the first step, Pt^{4+} ions could be bound to surface hydroxyl groups; then, they can interact with aluminum ions at the octahedral positions of β-Al_2O_3. The reduction of Pt^{4+} ions followed by the reduction and clustering of aluminum ions finally result in the formation of cationic vacancies on the surface of aluminum oxide.

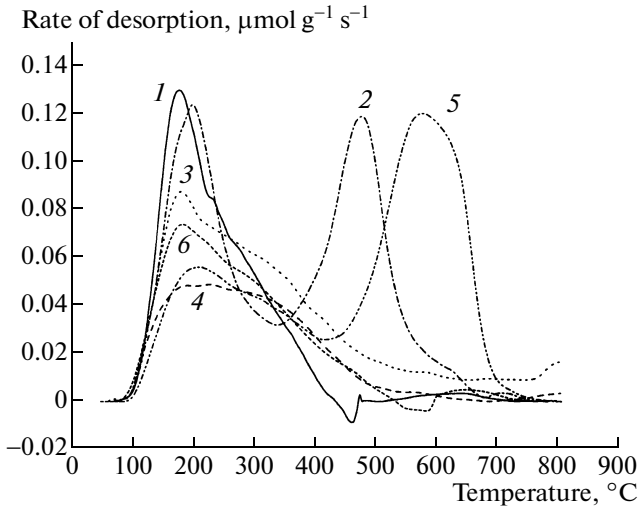

Fig. 6. Temperature-programmed desorption of ammonia from the surface of AP-64 catalyst samples. The numbers correspond to entries in Table 5.

The atomic radial distribution curves exhibited poorly resolved long-range fine structure peaks around platinum in the range of 3.5–4.5 Å (Fig. 5). It is believed that this range consists of a set of interatomic distances in disordered polyhedrons formed by platinum upon its interaction with coordinatively unsaturated sites of aluminum oxide.

The above allows us to expect that the formation of cationic vacancies due to the removal of aluminum atoms from the structure of alumina will enhance the acid properties of the surface.

Acid–Base Properties of the Alumina–Platinum Catalyst

The study of the TPD of ammonia from the surface of AP-64 catalyst samples subjected to various types of treatment (Fig. 6, Table 5) revealed acid sites corresponding to the activation energies of desorption $E_{des} < 130$ kJ/mol (weak and medium-strength acid sites) and ≥130 kJ/mol (strong acid sites).

As can be seen in Fig. 6, the TPD curve of ammonia for initial sample 1 (see Table 5) has a temperature maximum (at ~177°C). The high-temperature portion of the peak is expanded; in this case, a small peak was observed at ~470°C due to the desorption of hydrogen, which was formed upon the decomposition of ammonia at a platinum site at this temperature.

The behavior dramatically changed upon ammonia desorption from the surface of the catalyst reduced with hydrogen at 450°C and 50 atm but saturated with ammonia without thermal pretreatment (sample 2). The TPD curve (Fig. 6, curve *2*) exhibited two peaks

Table 5. Distribution of acid sites in terms of the activation energies of ammonia desorption on the AP-64 catalyst after various treatments

Entry	Pretreatment	Total number of sites, μmol/g	Number of sites (μmol/g) with E_{des}	
			<130 kJ/mol	≥130 kJ/mol
1	Initial sample pretreated with air at 500°C for 1 h	142	113 (79.7%)*	29 (20.3%)
2	Reduced with hydrogen at 450°C and 50 atm; TPD without thermal pretreatment	233	100 (42.9%)	133 (57.1%)
3	Reduced with hydrogen at 450°C and 50 atm, pretreated with H_2 (1 atm) for 1 h at 450°C	159	85 (53.5%)	74 (46.5%)
4	Initial sample reduced with H_2 (1 atm) for 12 h at 450°C	99	55 (55.6%)	44 (44.4%)
5	Reduced with hydrogen at 450°C and 50 atm, pretreated in H_2 (1 atm) at 450°C for 1 h; thereafter, saturated with water vapor for 0.5 h	242	58 (24.0%)	184 (76.0%)
6	Initial sample pretreated at 500°C with air for 1 h (1 atm) and then saturated with water vapor for 0.5 h	116	75 (64.7%)	41 (35.3%)

* The relative concentration of acid sites of the given type is specified in parentheses.

with T_{max} ~199 and 477°C. The low-temperature peak corresponds to $E_{des} < 130$ kJ/mol. It is close to the corresponding peak for sample 1 in terms of peak position and the number of sites. The high-temperature peak corresponds to acid sites with $E_{ads} > 130$ kJ/mol. The amount of these sites was ~57% of the total number of sites, which is greater than the number of these sites in the initial sample by a factor of 1.6.

Curves *3* and *4* in Fig. 6 reflect the desorption of ammonia from AP-64 reduced in hydrogen at 450°C and 50 atm for 12 h and pretreated in H_2 at 1 atm and the same temperature for 1 h before performing TPD (sample 3) or from the surface of the parent catalyst reduced in a flow of H_2 (12 h and 1 atm) immediately before saturation with ammonia (sample 4). The shapes of TPD curves for samples 3 and 4 were noticeably different. The amounts of adsorbed ammonia were also different. A pronounced peak with T_{max} ~ 180°C can be noted in the case of sample 3, whereas the curve for sample 4 exhibited no maximums. The fraction of strong sites in the above samples was close to 45%.

Based on the results of this experiment, we can conclude that the long-term treatment of the Pt/Al_2O_3 catalyst with hydrogen increased the number of strong acid sites. Their relative concentration was greater by a factor of ~2 than the corresponding value for similar sites on the surface of the parent unreduced catalyst.

It is well known that alumina, which serves as a support for platinum, contains both Brønsted and Lewis acid sites. It was demonstrated that long-term reduction generated strong aprotic sites on its surface. It is likely that the appearance of an intense peak in the TPD curve (Fig. 6, curve *2*) was related to the formation of acid sites of another nature on the catalyst surface. Indeed, quantum-chemical calculations [25] and the IR-spectroscopic and TPD studies of catalysts that adsorbed water and ammonia [26] demonstrated that the complexation of water molecules with the aprotic sites of zeolite Y resulted in the generation of strong Brønsted sites due to the polarization of O–H bonds in H_2O molecules. In this case, such a mechanism of the formation of an additional amount of strong Brønsted acid sites took place on the reduced catalyst. In this case, H_2O molecules formed in the course of catalyst reduction, as well as water eliminated from the alcohol upon its dehydration in the course of conversion by reaction (II), can serve as a source of water vapor.

This hypothesis was supported by the results of the TPD of ammonia from the surface of reduced AP-64, which was precalcined in a flow of H_2 (1 h at 450°C) and corresponded to sample 3 (Table 5), on which water vapor was adsorbed (also in a flow of hydrogen at a partial pressure of 4.57 Torr for 0.5 h at room temperature followed by blowing air for 0.5 h at 100°C) before ammonia. Note that both the average and the maximum activation energies of desorption from alumina for water were much higher than those of ammonia [27]. That is, in the course of NH_3 adsorption on the surface of hydrated AP-64, ammonia did not displace water molecules from adsorption sites and the observed TPD data characterized the strength distribution of Brønsted acid sites, the source of which were water molecules in this case. The results of the experiment are given in Fig. 6 (curve *5*) and Table 5 (sample 5). As can be seen in Fig. 6, as a result of water adsorption, a high-temperature peak with a maximum at 576°C was formed; this maximum corresponded to ammonia desorption from proton-donor sites. Note that this peak was shifted to the region of higher temperatures, as compared with the peak of sample 2. The average activation energy $\langle E_{des} \rangle$ of ammonia desorption from strong acid sites corresponding to the given peak was 190 kJ/mol, whereas it was as low as

~170 kJ/mol for sample 2. Hence, it follows that water molecules were primarily adsorbed at the strongest electron-acceptor sites of the sample freshly calcined in a flow of H_2, and they also formed strong proton-donor sites.

This conclusion was additionally supported by the following experiment: The initial AP-64 catalyst was subjected to oxidative pretreatment analogously to that performed with sample 1. Then, water vapor was adsorbed on the catalyst analogously to the case of sample 5: weakly bound water was removed at 100°C (for 0.5 h); the sample was cooled to room temperature and saturated with ammonia, and the TPD experiment was performed in accordance with a standard procedure. Figure 6 (curve *6*) shows the resulting TPD curve, and Table 5 summarizes the distribution of acid sites in terms of the activation energies of desorption. As can be seen in Fig. 6, the adsorption of ammonia on samples 1 and 6 and the shapes of their TPD curves were dramatically different. The desorption peak of hydrogen in sample 6 was shifted toward the region of high temperatures to ~600°C. The fraction of strong acid sites increased from 20.3 (initial catalyst without preliminary water adsorption) to 35.3% (sample 6). Correspondingly, the average activation energy of desorption from strong acid sites increased from 144 (sample 1) to ~150 kJ/mol (sample 6). The above data suggest that, in the case of the preliminary adsorption of water vapor on the oxidized catalyst (sample 1), the fraction of strong proton-donor acid sites did not sharply increase unlike the reduced prehydrated sample 5. However, the number of strong acid sites in sample 6 was greater than that in starting unhydrated sample 1 (Table 5).

Note that the palladium atoms are unlikely to be responsible for the formation of the great number of acid sites identified using the TPD of ammonia, because their concentrations are very low. It is believed that, after long-term reduction with hydrogen at 450°C, an additional amount of acid sites on the surface of the alumina–platinum catalyst was formed via the removal of surface lattice oxygen near the structural defects of γ-Al_2O_3.

This hypothesis was indirectly supported by X-ray diffraction data. After long-term reduction, the phase composition of the support remained unchanged (γ-Al_2O_3); however, the broadening of the Bragg reflections of the main crystallographic directions $d = 1.979$ and 1.396 Å increased by a factor of almost 2. It is well known that defects resulting in structural microdistortions are a factor affecting the broadening of reflections [28]. This hypothesis should be additionally tested.

CONCLUSIONS

The prolonged reduction of an alumina–platinum catalyst with hydrogen at an elevated temperature leads to the appearance of bifunctionality, as a result of which the selectivity of ethanol conversion dramatically changes: C_3–C_{10+} alkanes are formed from ethanol and diethyl ether. Experiments on the study of surface structure and acid–base properties demonstrated that the long-term reduction results in a considerable increase in the acidity of the catalyst; this facilitates the acceleration of reactions leading to the growth of a carbon skeleton in the products. Ethylene produced from ethanol is involved in this process. This results in an increase in the yield of normal alkanes. The recycling of the ethylene-containing gas leaving the reactor through a catalyst bed facilitates the development of this process.

Published data and the results of this work allow us to hypothesize that microphase surface changes occur in the course of long-term treatment with hydrogen at an elevated temperature; nanosized clusters of a platinum–aluminum intermetallide (Pt_2Al) are formed, and defects like anion vacancies that belong to strong aprotic acid sites are generated.

The interaction of these aprotic sites with water molecules, which are formed upon catalyst reduction, and with water adsorbed in the course of hydrothermal treatment leads to the formation of strong proton acid sites. Reaction (I) can also be a source of water for the generation of proton sites.

Ethanol, which undergoes dehydrogenation in reactions (III)–(VII) on platinum-containing sites, which may also participate in reaction (I), serves as a source of hydrogen required for the formation of alkanes (see reaction (I)).

Based on the experimental results, we can propose the following chemical reaction scheme for ethanol conversion in the course of reductive dehydration:

$$n[C_2H_5OH]_s \xrightarrow{AS} (n-x)[C_2H_4]_s \xrightarrow{AS} C_nH_{2n} \xrightarrow[+2[H]]{Pt} C_nH_{2n+2},$$
$$n[C_2H_5OH]_s \rightleftharpoons x(C_2H_5)_2O \rightarrow (n-x)[C_2H_4]_s$$

where AS refers to acid sites, and $[C_2H_4]_s$ is the substrate chemisorbed on the catalyst surface.

In accordance with the above scheme, ethanol undergoes dehydration with the formation of ethylene adsorbed on the catalyst surface, and this ethylene participates in the growth of a hydrocarbon chain. A portion of ethanol is consumed for the formation of diethyl ether, which is also converted into aliphatic hydrocarbons via reaction paths shown in the scheme, as found in this work. The hydrogenation of saturated

hydrocarbons into alkanes as the final products occurs at platinum-containing sites.

ACKNOWLEDGMENTS

This work was supported by the Russian Foundation for Basic Research (project no. 09-03-00133a).

REFERENCES

1. Mishchenko, G.L. and Vatsuro, K.V., *Sinteticheskie metody organicheskoi khimii* (Synthetic Methods in Organic Chemistry), Moscow: Khimiya, 1982.
2. Basagiannis, A.C., Panagiotopoulou, P., and Verykios, X.E., *Top. Catal.,* 2008, vol. 51, p. 2.
3. Rasko, J., Domok, M., Baan, K., and Erdohelyi, A., *Appl. Catal., A*, 2006, vol. 299, p. 202.
4. Erdohelyi, A., Rasko, J., Kecskes, T., Tooth, M., Domok, M., and Baan, K., *Catal. Today*, 2006, vol. 116, p. 367.
5. Tsodikov, M.V., Kugel', V.Ya., Yandieva, F.A., Kliger, G.A., Glebov, L.S., Mikaya, A.I., Zaikin, V.G., Slivinskii, E.V., Plate, N.A., Gekhman, A.E., and Moiseev, I.I., *Kinet. Katal.*, 2004, vol. 45, no. 6, p. 904 [*Kinet. Catal.* (Engl. Transl.), vol. 45, no. 6, p. 554].
6. Tsodikov, M.V., Yandieva, F.A., Kugel, V.Ya., Chistyakov, A.V., Gekhman, A.E., and Moiseev, I.I., *Catal. Lett.*, 2008, vol. 1, p. 25.
7. Chernyshov, A.A., Veligzhanin, A.A., and Zubavichus, Y.V., *Nucl. Instrum. Methods Phys. Res., Sect. A*, 2009, vol. 603, p. 95.
8. Yushchenko, V.V., *Zh. Fiz. Khim.*, 1997, vol. 71, no. 4, p. 628 [*Russ. J. Phys. Chem.* (Engl. Transl.), vol. 71, no. 4, p. 547].
9. Ravel, B. and Newville, M., *J. Synchrotron Radiat.*, 2005, vol. 12, p. 537.
10. Ankudinov, A.L., Ravel, B., Rehr, J.J., and Conradson, S.D., *Phys. Rev. B: Condens. Matter*, 1998, vol. 58, p. 7565.
11. Ostromyslenskii, I.I., *Zh. Russ. Fiz.-Khim. O–va.*, 1915, vol. 47, p. 1494.
12. Lebedev, S.V., *Zh. Org. Khim.*, 1933, vol. 3, p. 698.
13. Sykes, P., *A Guide Book to Mechanism in Organic Chemistry*, New York: Wiley, 1981.
14. Shuikin, N.I. and Bel'skii, I.F., *Dokl. Akad. Nauk SSSR*, 1958, vol. 120, no. 3, p. 548.
15. Liberman, A.L., Bragin, O.V., and Vasina, T.V., *Izv. Akad. Nauk SSSR, Ser. Khim.*, 1963, no. 7, p. 1352.
16. Chattopadhyay, T. and Schubert, K., *J. Less-Common Met.*, 1976, vol. 45, p. 79.
17. Duplyakin, V.K., Belyi, A.S., Ostrovskii, N.M., Smolikov, M.D., Chelganov, E.M., and Nizovskii, A.I., *Dokl. Akad. Nauk SSSR, Fiz. Khim.*, 1989, vol. 305, no. 3, p. 648.
18. Matyshak, V.A., Khomenko, T.I., Bondareva, N.K., Panchishnyi, V.I., and Korchak, V.N., *Kinet. Katal.*, 1998, vol. 39, no. 1, p. 100 [*Kinet. Catal.* (Engl. Transl.), vol. 39, no. 1, p. 93].
19. Belyi, A.S., *Kinet. Katal.*, 2005, vol. 46, no. 5, p. 728 [*Kinet. Catal.* (Engl. Transl.), vol. 46, no. 5, p. 684].
20. Kang, J.H., Menard, L.D., Nuzzo, R.G., and Frenkel, A.I., *J. Am. Chem. Soc.*, 2006, vol. 128, p. 12 068.
21. Hayek, K., Goller, H., Penner, S., Rupprecher, G., and Zimmerman, C., *Catal. Lett.*, 2004, vol. 92, p. 1.
22. Stadelmann, P., *Ultramicroscopy*, 1987, vol. 21, p. 131.
23. Zhong, X., Zhu, J., and Liu, J., *J. Catal.*, 2005, vol. 236, p. 9.
24. Petraszek, A., Costa, P.D., Markues, R., Kornelak, P.., Hansen, T.W., Carma, J.., and Najbar, M., *Catal. Today*, 2007, vol. 119, p. 187.
25. Tikhii, V., Kubasov, A.A., and Stepanov, N.F., *Zh. Fiz. Khim.,* 2003, vol. 77, no. 9, p. 1620 [*Russ. J. Phys. Chem.* (Engl. Transl.), vol. 77, no. 9, p. 1455].
26. Kubasov, A.A., Kitaev, L.E., Yushchenko, V.V., and Tikhii, Ya.V., *Vestn. Mosk. Univ., Ser. 2: Khim.*, 2005, vol. 46, no. 4, p. 236.
27. Yushchenko, V.V. and Romanovskii, B.V., *Zh. Fiz. Khim.*, 1997, vol. 71, no. 11, p. 2048 [*Russ. J. Phys. Chem.* (Engl. Transl.), vol. 71, no. 11, p. 1852].
28. JCPDF-ISDD 1999, card 29-0063.